LETTER • **OPEN ACCESS**

Intra-cavity measurement concept of dispersion properties with a tunable fiber-integrated laser

OPEN ACCESS
IOP Publishing | Astro Ltd
Laser Physics Letters
Laser Phys. Lett. **16** (2019) 025101 (7pp)
https://doi.org/10.1088/1612-202X/aaf78e

Letter

Intra-cavity measurement concept of dispersion properties with a tunable fiber-integrated laser

Tobias Tiess[1], Alexander Hartung[1], Martin Becker[1], Christoph Chojetzki[2], Manfred Rothhardt[1], Hartmut Bartelt[1,3] and Matthias Jäger[1]

[1] Leibniz Institute of Photonic Technology, Albert-Einstein-Str. 9, 07745 Jena, Germany
[2] FBGS Technologies GmbH, Winzerlaer Str. 2, 07745 Jena, Germany
[3] Abbe Center of Photonics, Friedrich Schiller University Jena, Albert-Einstein-Str. 6, 07745 Jena, Germany

E-mail: tobias.tiess@leibniz-ipht.de

Received 5 October 2018
Accepted for publication 26 November 2018
Published 4 January 2019

Abstract

The dispersion properties of fibers depict a key characteristic to model the propagation of ultra-short pulses in waveguides. In the following, a new method is presented to directly measure the dispersion properties of fibers and optical components in the time domain. The analysis is based on pulse shape variations along the tuning range of a theta cavity fiber laser (TCFL) depending on the adjusted repetition rate. The automated measurement procedure, evaluating pulse symmetry, achieves a temporal sensitivity below 5 ps surpassing the resolution of the acquisition electronics. Exemplarily, two samples of Nufern PM980-XP fiber are investigated with an Yb-doped tunable TCFL retrieving the mean dispersion parameter D_λ by comparative measurements. The obtained results are compared to a reference method based on spectral interferometry. With deviations in D_λ between either approach of 0.3% and 1.3%, respectively, the results agree well within the measurement errors of the TCFL, verifying the presented concept. Due to the pulse formation process extending over multiple round trips, this approach achieves an enhanced sensitivity compared to competing direct temporal methods. Together with an alignment free operation, the fiber-integrated TCFL depicts a simple and robust concept showing potential in specific measurement scenarios such as in quality management.

Keywords: fiber lasers, tunable laser, fiber Bragg grating, disperion

(Some figures may appear in colour only in the online journal)

1. Introduction

The dispersion properties of optical fibers govern the behavior of pulses propagating in a system. With the rise of mode-locked fiber lasers generating pulse durations in the picosecond and femtosecond scale with an extended spectral bandwidth, the measurement of the dispersion behavior of optical components has created growing attention. One of the fundamental design challenges in pulsed light sources concerns the dispersion management [1]. The overall cavity round-trip dispersion dictates the pulse formation process setting the operation regime of ultrashort pulsed lasers [2–4]. In addition, tailored dispersion designs enable fibers to drive subsequent spectral broadening and simultaneous pulse compression down

to the single-cycle regime for enhanced peak powers [5, 6]. Harvesting the full potential of nonlinear interactions in waveguides, fiber-based supercontinuum generation is governed by the dispersion properties accessing multi-octave spanning emission bandwidths [7–9]. On the other side, specific fibers in telecommunication are designed with relatively low dispersion to suppress pulse broadening, limiting the bandwidth in data transition [10].

The propagation speed of a pulse is governed by the group velocity v_{gr} given by

$$v_{gr} = \frac{d\omega}{d\beta} = c_0 \left(n_{eff} - \lambda \frac{dn_{eff}}{d\lambda} \right)^{-1} \tag{1}$$

with c_0 as the speed of light in vacuum, ω as the radial frequency, λ as the wavelength and $\beta(\omega)$ as the dispersive propagation constant of the fundamental mode in the waveguide with effective mode index $n_{eff}(\omega) = \lambda\beta(\omega)/(2\pi)$. In order to model the propagation effects of pulsed signals with considerable bandwidth, the spectral dependency in v_{gr} needs to be considered. It is determined by the dispersion properties of the fiber (including the contribution of material dispersion as well as the waveguide dispersion). They are usually described by the dispersion parameter D_λ defined as

$$D_\lambda = -\frac{\lambda}{c_0} \frac{d^2 n_{eff}}{d\lambda^2} = -\frac{2\pi c_0}{\lambda^2} \beta_2 \tag{2}$$

with $\beta_2 = d^2\beta/d\omega^2$ depicting the group velocity dispersion (GVD). In an illustrative picture, D_λ denotes the dispersion-caused temporal delay experienced by a traveling signal per spectral bandwidth and per propagation distance in a fiber. Depending on the sign, the system operates in the normal dispersion regime ($D_\lambda < 0$) or the anomalous dispersion regime ($D_\lambda > 0$) inducing fundamentally different effects in pulse formation.

Due to their significance for the design of pulsed light sources, experimental methods are required to measure the dispersion properties of fibers and characterize optical modules. Most concepts rely on an indirect interferometric measurement [11–13], such as in white light interferometry [14] or spectral phase interferometry [15]. While they usually require only short lengths of fibers (<1 m) and operate over extended bandwidths, they employ elaborate analysis procedures to retrieve the fiber dispersion. Additionally, interferometric approaches are prone to environmental influences demanding protected lab conditions. On the other side, a direct temporal measurement is known based on the pulse delay technique [16]. The difference in propagation time through the fiber for pulses at various wavelengths is measured corresponding to the dispersion characteristics. This robust method enables quick and direct assessment of dispersion properties. Due to the small time scales, hundreds of meters or even kilometers of fiber length are required (temporal resolution in the range of 50 ps) [17].

In this paper, we present a novel temporal method to directly measure the dispersion properties of fibers and fiber modules. It relies on pulse shape variations observed in a tunable theta cavity fiber laser (TCFL) [18, 19] along its spectral operation window. Due to the pulse formation process over several round trips in the laser, this approach features an enhanced temporal sensitivity reducing the length of the required fiber samples. After the underlying concept of the tunable TCFL is introduced, the observed pulse shape variations are discussed, providing the foundation to analyze the total cavity dispersion of the laser. Accordingly, an automated procedure is developed to retrieve the dispersion properties of fiber samples by comparative measurements. As an example, two fibers under test (FUT) from different batches of the model `Nufern PM980-XP` are studied with this new concept. In order to provide an experimental reference, the obtained values for D_λ are compared to an alternative method characterizing the dispersion properties based on spectral interferometry.

2. Concept of tunable theta cavity fiber laser (TCFL)

The tunable TCFL depicts a concept to discretely tune the emission wavelength of a pulsed fiber-integrated laser based on an FBG array as monolithic filter. It comprises N different FBGs at dissimilar feedback wavelengths $\lambda_{FBG,i}$, respectively, that are spaced with a spatial separation Δz along the fiber axis (see figure 1). The discrete sampling uniquely facilitates tailored spectral filter responses, enabling large tuning bandwidths as well as customized emission wavelengths. The theta layout fuses the distributed feedback from this filter structure with a constant pulse repetition rate along the tuning range of the laser. The principles of this tuning concept are elucidated in detail in [18]. A brief overview is given in the following.

The principle setup of the TCFL is sketched in figure 1. The theta resonator comprises an outer ring structure with the active fiber as gain element, a pump coupler to inject the pump light, an output coupler to extract the laser signal, and two circulators to ensure unidirectional operation as well as to couple the signal to a bidirectional middle branch. This part incorporates the FBG array as reflective spectral filter and an acousto-optic modulator (AOM) driven by an electrical pulse generator (in the experiment: `Tektronix AWG3252C`). It pulses the system as well as controls the emission wavelength λ_L via optical gating. Additionally, some delay fiber can be added, e.g. for investigating its dispersion properties (FUT) as discussed in this work.

The laser signal interacts twice per round trip with the FBG array (firstly when injected from circulator 1, secondly when injected from circulator 2) in a counter-propagating fashion balancing the wavelength dependent pulse delays induced by the distributed filter feedback. The tuning mechanism of the TCFL relies on optical gating with an AOM to lock laser oscillations to a specific grating out of the ensemble provided by the FBG array, determining λ_L. During the second filter interaction, the AOM presets the time of flight of laser pulses in the FBG array by two consecutive optical transmission windows. Whereas the first window per round trip injects the signal to the filter section, the second window picks out the response from a specific grating i ($i \in \mathbb{N}, i \leqslant N$). Operating as spectral tuning parameter, the adjustable delay τ_{1-2} between both transmission gates determines the time of flight in the filter section controlling its effective feedback wavelength $\lambda_{FBG,i}$. Applying the optical gating signal with a modulation period

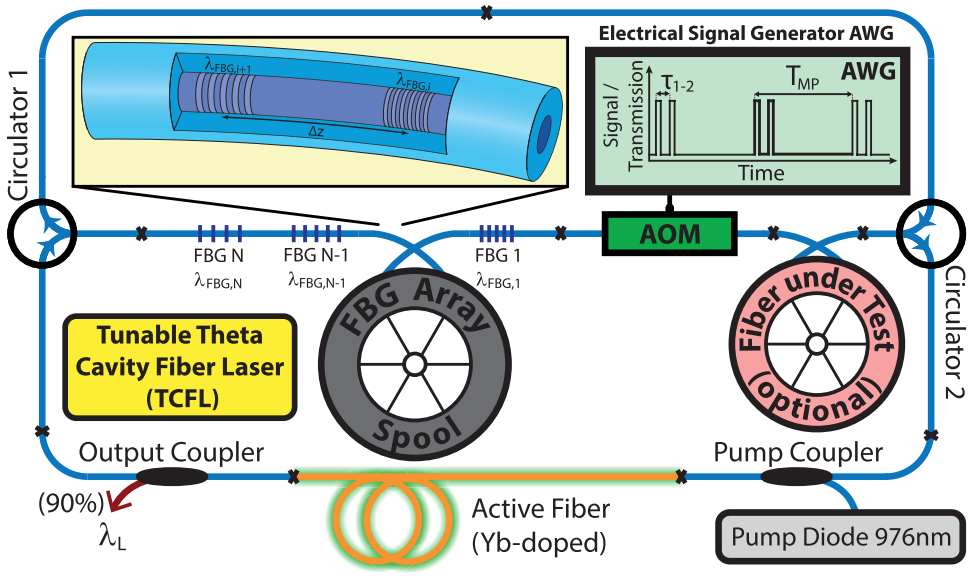

Figure 1. Principle experimental setup of the tunable Yb-doped TCFL. A discrete FBG array is used as reflective spectral filter. Optical gating for controlling the emission properties (e.g. emission wavelength λ_L) is realized with an AOM controlled by a LabVIEW driven electrical signal generator (AWG). The fiber-integrated setup is implemented in a polarization-maintaining (PM) layout. For the dispersion measurement concept, the FUT is spliced between circulator 2 and the AOM.

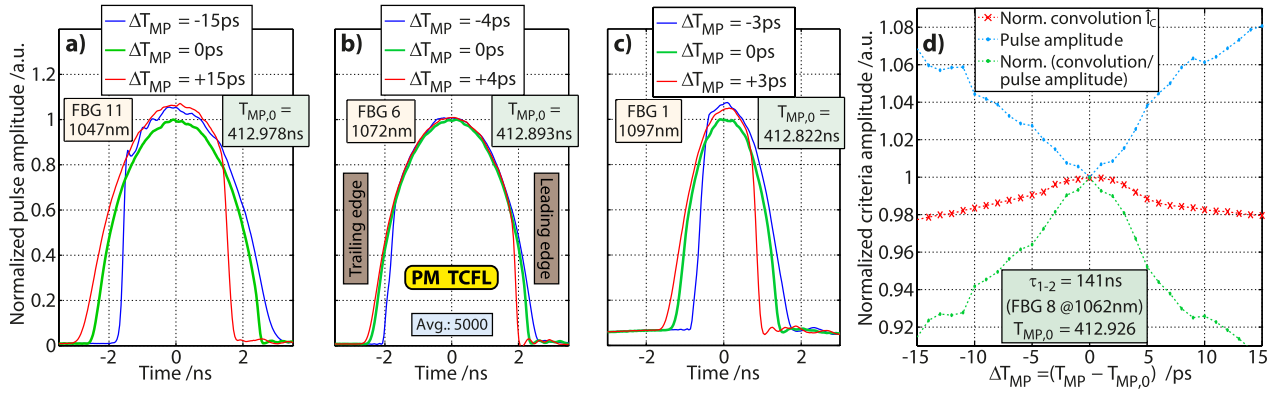

Figure 2. Graph (a) plots pulse shapes emitted by the PM TCFL locked to FBG 11 (beginning of spectral tuning range). The three traces correspond to three different modulation periods T_{MP} indicated by the detuning $\Delta T_{MP} = T_{MP} - T_{MP,0}$. The central modulation period $T_{MP,0}$ at FBG 11 ($\lambda_L = 1047$ nm) ensures symmetric parabola-like pulses whereas detuning $\Delta T_{MP} \neq 0$ ps causes steepening on either side. Graphs (b) and (c) show corresponding features measured at FBG 6 at $\lambda_L = 1072$ nm (center of tuning range) and FBG 1 at $\lambda_L = 1097$ nm (end of tuning range). With the changing emission wavelengths from graph (a)–(c), the central modulation period $T_{MP,0}$ decreases by 156 ps. Plot (d) compares three exemplary features to quantify the pulse shape variations with T_{MP} computed for a measurement at $\lambda_L = 1062$ nm (FBG 8). The blue trace tracks the normalized pulse amplitude, the red trace the normalized self-convolution and the green trace a combined value dividing the normalized self-convolution by the corresponding normalized pulse amplitude. The extrema in each curve coincide at $T_{MP} = T_{MP,0}$.

of T_{MP} matching the pulse round trip time in the TCFL, laser pulses are generated over multiple round trips at $\lambda_L = \lambda_{FBG,i}$.

The experimental investigations in this work were conducted with a polarization-maintaining (PM) TCFL layout. The FBG array comprises 11 FBGs with a reflectivity of 90% –95% equidistantly covering the spectral range from 1047 nm to 1097 nm.

3. Pulse shape variations along the tuning range

While the theta-ring layout with the two counter-propagating filter interactions ensures a constant physical resonator length L for each wavelength (despite the distributed filter feedback, assuming steady FBG characteristics), dispersion effects affect the group velocity v_{gr}, inducing a marginal spectral dependency of the actual pulse round trip time over the tuning range. Its magnitude correlates with the total cavity dispersion of the TCFL.

Whereas the TCFL can be operated typically with a constant modulation period neglecting the effects of dispersion, the detailed pulse shape depends on the mismatch ΔT_{MP} between the modulation period T_{MP} and the precise pulse round trip time, evolving along the tuning range. This effect is pictured in figures 2(a)–(c). Graph (a) plots three averaged pulse shapes emitted by the PM TCFL locked to FBG 11 ($\lambda_L = 1047$ nm) for slightly varying T_{MP}. The green trace indicates a symmetric parabola-like pulse shape. In this case,

the system is operated at the default modulation period $T_{MP,0}$ ($\Delta T_{MP} = 0$ ps) matching the actual round trip time in the resonator. In contrast, detuned modulation periods ($|\Delta T_{MP}| > 0$ ps) induce asymmetric steepening to either side of the pulse. Due to repetitive pulse clipping over multiple round trips at the temporal AOM gate, the leading edge steepens in case of $\Delta T_{MP} > 0$ ps ($T_{MP} > T_{MP,0}$, red trace). For the inverse case of $\Delta T_{MP} < 0$ ps (blue trace), steepening is observed at the trailing edge. Graphs (b) and (c) depict the same scenario measured at different emission wavelengths of the laser system along its tuning range. $T_{MP,0}$, ensuring parabola-like pulses, is readjusted for each λ_L. The evolution in $T_{MP,0}$ along the tuning range correlates with the dispersion properties of the cavity.

As graph (a)–(c) confirm, the pulse shape variations feature a temporal sensitivity in the lower picosecond range with respect to the adjusted T_{MP}. Due to the pulse formation process over multiple round trips in the laser, the sensitivity is superior to the applied acquisition electronics (bandwidth of oscilloscope: 6 GHz; bandwidth and photodiode: 5 GHz, joint temporal resolution >100 ps) enabling the measurement of short fiber lengths.

For further analysis, a quantitative measure is required to evaluate the pulse shape variations and objectively track down $T_{MP,0}$ along the tuning range of λ_L. Comparing the pulse characteristics in figures 2(a)–(c), two main features may be utilized: while detuning in T_{MP} induces asymmetric steepening on either edge of the pulse, this effect also causes mildly increasing amplitudes due to pulse shortening. The symmetry in the pulse shape $\mathrm{Pulse}(t)$ is quantified by a normalized self-convolution function $I_C(t)$ as defined by

$$I_C(t) = \frac{\int_{-\infty}^{+\infty} \mathrm{Pulse}(\tau) \cdot \mathrm{Pulse}(t-\tau) d\tau}{\int_{-\infty}^{+\infty} \mathrm{Pulse}(t) \cdot \mathrm{Pulse}(t) dt}. \qquad (3)$$

Whereas the denominator depicts a normalization factor, the negative τ for the second factor in the nominator reverses the pulse shape so that the integral is maximized for highest symmetry in Pulse(t). The integration borders are formally given by $-\infty$ and $+\infty$. In the experimental study, the function is limited by the length of the recorded trace in $\mathrm{Pulse}(t)$.

Figure 2(d) compares the different criteria to analyze the pulse shapes. For an exemplary λ_L of 1062 nm (FBG 8), the temporal emission behavior of the TCFL has been recorded along an incrementally scanned T_{MP} (step size: 1 ps). As expected, $I_C(\Delta T_{MP})$ (red trace) peaks at $\Delta T_{MP} = 0$ ps indicating maximized symmetry in the pulse shape at $T_{MP,0}$. Correspondingly, the normalized pulse amplitude (blue trace) features a minimum. A third criterion has been evaluated by the green trace dividing the red trace (convolution criteria) by the blue trace (pulse amplitude criteria) showing enhanced sensitivity (steeper slopes). While all three criteria enable an automated acquisition of $T_{MP,0}$ for a given emission wavelength, only the normalized convolution criterion featured a monotonic behavior towards the extrema throughout the complete study. Thus, despite the lower sensitivity, it is employed as robust criterion to quantify the pulse shape variations defining $T_{MP,0}$ at its maximum.

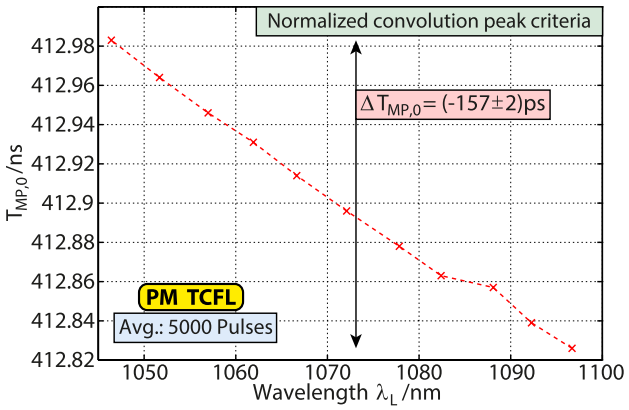

Figure 3. The plot captures the drift in $T_{MP,0}$ along the tuning range of the TCFL caused by the total cavity dispersion.

Recording the maximum $\widehat{I_C} = I_C(T_{MP,0})$ of $I_C(T_{MP})$ along the tuning range of the TCFL enables to track down the dispersion caused evolution of $T_{MP,0}$. A `LabVIEW` driven control software has been implemented to automate the scan procedure. A corresponding measurement along the 11 emission wavelengths of the TCFL is highlighted in figure 3. Along the tuning range $\delta\lambda_L$ of 50 nm, the pulse round trip time decreases by $\Delta T_{MP,0} = -157$ ps caused by the overall cavity dispersion. This value agrees well with the observed shift from figures 2(a)–(c) ($\Delta T_{MP,0} = -156$ ps). The trace in figure 3 follows an almost linear relation. Only the value at $\lambda_L = 1087$ nm (FBG 3) deviates caused by a measurement artifact due to a deviating FBG reflectivity. The corresponding grating features a lower reflectivity by about 5% compared to the surrounding FBGs slightly increasing the penetration depth [20]. Due to the comparative measurement procedure later on, this effect is balanced out.

From the retrieved value $\Delta T_{MP,0} = -157$ ps , the average dispersion of the fibers in the cavity can be computed with the relation

$$D_\lambda = \frac{\Delta T_{MP,0}}{L \cdot \delta\lambda_L}. \qquad (4)$$

The resonator length can be approximated from the pulse round trip time $T_{MP} \approx 413$ ns, giving $L \approx 85$ m ($n_{eff} \approx 1.45$ for silica glass). Accordingly, the effective cavity dispersion for the fibers is estimated to $D_\lambda = 37$ ps $(\mathrm{nm} \cdot \mathrm{km})^{-1}$, matching well to typical dispersion values of step-index SM fibers at 1 μm (`Corning HI1060`: $D_\lambda = 38$ ps $(\mathrm{nm} \cdot \mathrm{km})^{-1}$ [21]). Accordingly, the shift in $T_{MP,0}$ along the tuning range is driven by the dispersion properties of the fibers in the cavity.

4. Measurement of dispersion properties

The high sensitivity of pulse shape variations regarding the actual T_{MP} in the TCFL provides the foundation to determine the total cavity dispersion. By applying comparative measurements, this effect is exploited to retrieve the dispersion properties of optical fibers and components. The automated measurement procedure will be discussed based on the

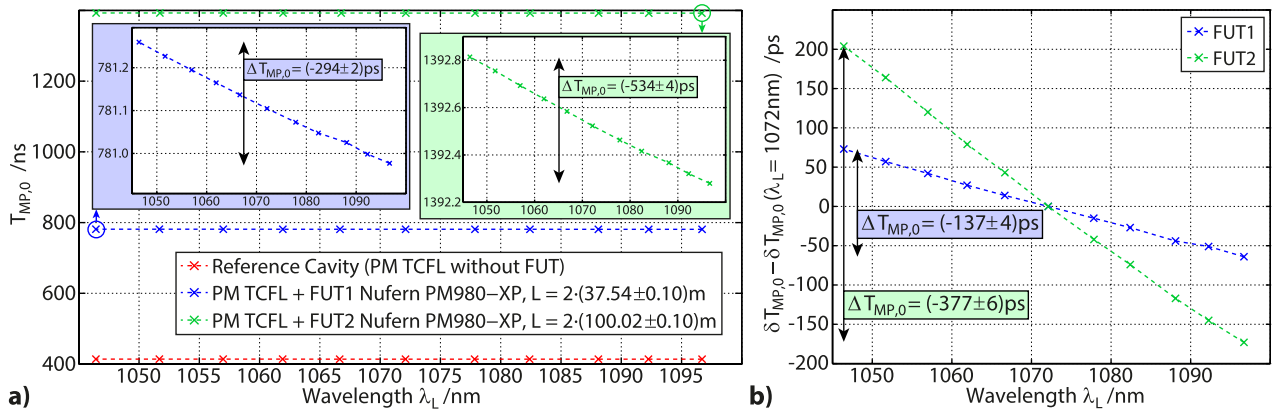

Figure 4. The graphs analyze the evolution of $T_{MP,0}$ over the tuning range for two FUT samples. Graph (a) shows the measured $T_{MP,0}$ for the PM TCFL in the reference layout as well as with two FUT samples. Two inset graphs highlight the detailed trace for FUT1 (blue) and FUT2 (green). Plot (b) pictures the evaluated relative change $\delta T_{MP,0}$ by subtracting FUT1 or FUT2 from the reference measurement. By also subtracting $\delta T_{MP,0}$ ($\lambda_L = 1072$ nm) measured at FBG 6 (considers the mean change in $T_{MP,0}$ due to the additional fiber length), the plain dispersion effect is isolated for FUT1 ($\Delta T_{MP,0} = (-137 \pm 4)$ ps) and FUT 2 ($\Delta T_{MP,0} = (-377 \pm 6)$ ps). The error bars are estimated from the convolution curves considering their slopes as well as reproducibility.

investigation of two fibers under test FUT1 and FUT2. Both samples originate from different batches of the fiber model `Nufern PM980-XP` (core/cladding diameter: 5.5/125 μ m, $NA = 0.12$, Panda geometry), which is widely employed in low-power fiber lasers, telecommunications and sensing. They exhibit different lengths (FUT1: $L = (37.54 \pm 0.10)$ m; FUT2: $L = (100.02 \pm 0.10)$ m, measured with a fiber spooling machine) to study the sensitivity of the concept.

To analyze the dispersion of a specific fiber under test (FUT) in the TCFL, two comparative experiments are conducted. In a first step, the plain TCFL is analyzed regarding its total cavity dispersion (reference measurement). Subsequently, the FUT is spliced into the cavity (operating in the slow axis), for instance between circulator 2 and the AOM (see figure 1). This utilizes a double pass arrangement for higher sensitivity, requiring shorter fiber lengths. The expanded TCFL with the FUT is scanned again determining its overall dispersion properties. By subtracting the shifts in $T_{MP,0}$ between both measurements, the net dispersive response from the FUT can be retrieved.

These measurements are depicted in figure 4. Graph (a) shows the measured $T_{MP,0}$ for the reference cavity (plain TCFL without FUT, red trace) as well as the extended cavities with FUT1 (blue trace) and FUT2 (green trace). Due to the different resonator lengths of the three configurations, the traces are offset to each other. Whereas the shift of $T_{MP,0}$ for the red trace is already highlighted in figure 3, two insets in figure 4(a) zoom in on the evolution of $T_{MP,0}$ in the blue and green trace. Due to the longest fiber length of FUT2, the green trace shows the strongest dispersive response with a shift in $T_{MP,0}$ of 534 ps.

By subtracting the red trace from the blue and the green trace, respectively, the net dispersive response from the different FUT samples is extracted. This is shown in figure 4(b) plotting the corresponding differences $\delta T_{MP,0}$. Both traces are also corrected for a constant offset ($\delta T_{MP,0}$ at $\lambda_L = 1072$ nm) to compare them in the same scale. In both cases, the pulse round trip time declines because of the normal dispersion of the fiber

Table 1. Experimental results of dispersion measurements with the TCFL ($D_{\lambda,exp.}$) including a comparison to an alternative method [13] ($D_{\lambda,exp.2}$). For the latter, error bars are estimated from the standard deviation of a polynomial fit (3rd order) to the obtained D_λ values.

Symbol	FUT1	FUT2
L	$2 \cdot (37.54 \pm 0.10)$ m	$2 \cdot (100.02 \pm 0.10)$ m
$\delta\lambda_L$	(50.27 ± 0.04) nm	(50.27 ± 0.04) nm
$\Delta T_{MP,0}$	(-137 ± 4) ps	(-377 ± 6) ps
$D_{\lambda,exp.}$	(-36.3 ± 1.2) ps (nm · km)$^{-1}$	(-37.5 ± 0.7) ps (nm · km)$^{-1}$
Error	3.3%	1.9%
$D_{\lambda,exp.2}$	(-36.4 ± 0.3) ps (nm · km)$^{-1}$	(-37.0 ± 0.3) ps (nm · km)$^{-1}$

samples. Due to the longer length of FUT2, the sole dispersive response is stronger inducing a shift of $\Delta T_{MP,0} = (-377 \pm 6)$ ps (FUT1: $\Delta T_{MP,0} = (-137 \pm 4)$ ps). The error bars are estimated from the convolution curves $I_C(T_{MP})$ by evaluating reproducibility and slope. For the red and blue curve, they match the sampling density of 1 ps in the scan of T_{MP}. Based on (4) and the obtained values for $\Delta T_{MP,0}$, the mean dispersion parameter for both FUT samples can be calculated along the tuning range by a linear approximation. The results are summarized in table 1. The effective fiber lengths L are doubled due to the double-pass configuration of the FUT in the middle branch.

Whereas the analysis for FUT1 results in $D_{\lambda,exp.} = (-36.3 \pm 1.2)$ ps (nm · km)$^{-1}$, FUT2 gives a 3.3% larger value of $D_{\lambda,exp.} = (-37.5 \pm 0.7)$ ps (nm · km)$^{-1}$. Due to the longer sample length inducing a stronger dispersive response, the relative error of the latter measurement is smaller reaching 1.9% (FUT1: 3.3%). Even though the values for both FUT overlap with each other considering the error bars, the deviation was measured reproducibly. Additionally, the data sheets of both fiber samples record a different mode field diameter (MFD). While FUT1 is listed with a MFD value of 7.1 μm, FUT2 features a smaller MFD of 6.6 μm (both

measured at 980 nm), which may cause a stronger waveguide dispersion contribution.

Because reference values are hardly found in literature, a reference method has been implemented based on spectral interferometry [13] to characterize both FUT samples and clarify the origin of the deviation between the obtained $D_{\lambda,exp.}$ values. The free-space coupled approach in [13] has been adapted by using a supercontinuum light source and by realizing the setup in a PM layout at the wavelength band around 1 μm including a fiber-pigtailed polarizer in the branch of the light source. Both FUT are measured with this approach using about 40 cm long samples. The retrieved values for $D_\lambda(\lambda)$ are fitted with a 3rd order polynom to determine the mean $D_{\lambda,exp.2}$ with respect to the spectral operation window of the TCFL. The measurement error is estimated by the standard deviation of the fit. The results for both FUT samples are attached in table 1. With deviations of 0.3% (FUT1) and 1.3% (FUT2), they agree very well with the results obtained with the TCFL, verifying the presented analysis concept. Relying on an indirect measurement in the spectral domain, the reference method also indicates $|D_\lambda|$ to be larger for FUT2, but the measurement accuracy does not allow for definite conclusions.

In the last step, the approach of the TCFL is investigated regarding the spectral resolvability in $D_{\lambda,exp.}$. Whereas similar results have been obtained for FUT2, figure 5 presents the investigation for FUT1. In principle, the implemented TCFL is tunable over 50 nm providing up to 11 emission lines λ_L to evaluate spectrally resolved data. In this case, (4) is evaluated incrementally along the tuning range, analyzing $\Delta T_{MP,0}$ over fractional spectral bands of width $\delta\lambda_L$. The results are illustrated in figure 5. While the red cross presents the mean $D_{\lambda,exp.}$ over the full operation bandwidth as discussed before, the orange trace evaluates D_λ over spectral bands of $\delta\lambda_L = 25$ nm (i.e.: at FBG 1, 6 and 11), and the violet trace over $\delta\lambda_L = 10$ nm (i.e.: FBG 1, 3, 5, 7, 9, 11). The legends also list the corresponding measurement errors. Since the absolute errors do not change, the relative errors increase for smaller evaluation bandwidths in D_λ. The graph also plots the results obtained with the experimental reference method [13] (gray dots) including the polynomial fit (dark gray trace). For comparison, a numerical analysis has also been performed by a spectrally resolved modal analysis based on COMSOL Multiphysics® software assuming a plain step-index fiber model (green trace).

Whereas the numerical trace clearly deviates from the experimental results, indicating a oversimplified model (e.g.: ideal step-index profile) or deviating fiber specifications, the experimental traces agree well within the corresponding errors. However, due to the increasing measurement errors, detailed spectral conclusions cannot be drawn from the TCFL measurement. This is especially highlighted for the violet trace showing an unphysical zick-zack shape. Still the TCFL indicates the same deviation from the numerical model as the reference method in the dark gray trace. The limited spectral resolution could be partly overcome by also applying a polynomial fit assuming slowly evolving features.

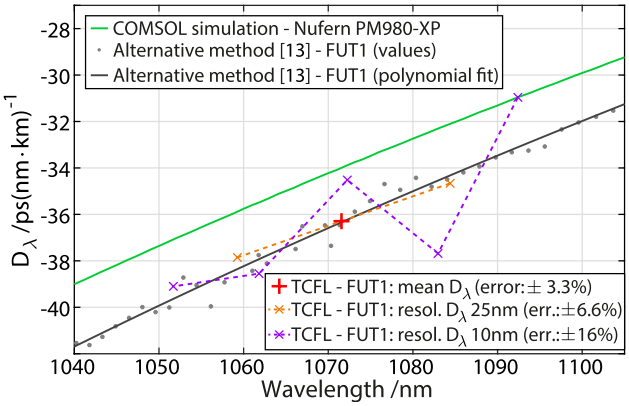

Figure 5. The plot shows the measured dispersion parameter D_λ for different spectral resolutions (resol.) applying the TCFL and FUT1. An experimental reference is provided by the gray dots that are recorded with an alternative method based on spectral interferometry [13]. The dark gray trace represents the corresponding polynomial fit (3rd order). The graph also includes simulation results (green trace) based on the released specifications of the fiber Nufern PM980-XP obtained via a modal analysis with COMSOL Multiphysics®.

5. Conclusion

A new method has been presented for a direct measurement of dispersion properties of fibers and fiber modules in the time domain. The automated approach is based on evaluating pulse shape variations along the tuning range of a discretely tunable TCFL, revealing the cavity dispersion. The applicability of the concept has been demonstrated by studying two fiber samples FUT1 and FUT2 of the fiber model Nufern PM980-XP. The experiment delivered mean dispersion parameters of $D_{\lambda,exp.} = (-36.3 \pm 1.2)$ ps (nm · km)$^{-1}$ (FUT1) and $D_{\lambda,exp.} = (-37.5 \pm 0.7)$ ps (nm · km)$^{-1}$ (FUT2) that agree well with a reference method based on spectral interferometry, which deviated by 0.3% and 1.3%, respectively. The measurement with the TCFL even indicates a deviation between the characteristics of FUT1 and FUT2, which may arise from deviating batch specifications. A measurement error as small as 1.9% has been achieved. With the excellent agreement between both experimental methods, the presented temporal measurement concept with the TCFL has been verified.

In any case, the elements under test (e.g. FUT) need to satisfy a few conditions to be suitable for this dispersion measurement approach. Most notably, they need to feature reasonable insertion losses to sustain laser operations in the TCFL. With round trip losses between 15 dB to 20 dB in the plain resonator, additional losses by the FUT in the same magnitude could be tolerated. Also partly connected to the losses, the FUT needs to be available with reasonable length. Due to the direct temporal measurement with limited sensitivity (in the experiment: $\geqslant 1$ ps), the minimum detectable length is in the range of a few meters. Assuming an exemplary FUT with $D_\lambda = 40$ ps (nm · km)$^{-1}$, a tuning range of $\delta\lambda_L = 50$ nm and an effective delay due to the dispersive distortion of $\Delta T_{MP,0} \geqslant 10$ ps for a profound measurement, the minimum length for the FUT is about 5 m. Compared to the previously mentioned pulse delay technique [16] working with hundreds

of meters or even kilometers of FUT, this is a significantly shorter length of fiber to draw conclusions about the dispersive character with a direct measurement in the time domain. Absolute measurement accuracies in the picosecond scale are demonstrated in the experiment without using high-end detection electronics. The enhanced temporal sensitivity arises from the pulse formation process over multiple round trips in the laser.

Still, the plain temporal measurement with the TCFL may not outperform the spectral resolution and accessible bandwidth of common dispersion analysis concepts relying on spectral interferometry as well as broadband supercontinuum sources [22]. Nevertheless, this approach establishes a simple measurement of pulse shape features to directly retrieve the dispersion properties for fiber modules and laser resonators. The fiber-integrated setup ensures robust and reliable operation without alignment requirements. Hence, for spliceable components, the TCFL provides direct and easy access to the dispersion characteristics. With a suitable setup, multiple components may be quickly investigated for their coarse dispersion characteristics, e.g. in quality management categorizing their performance. Even solely analyzing the temporal delays in the resonator (without retrieving D_λ) enables swift conclusions to be drawn about the dispersion regimes. Additionally, with the measurement concept relying on laser operations, corresponding specialty fibers can be analyzed with reasonable lengths. For instance, PM components can be studied in their operating axis. Furthermore, the dispersion magnitude of active fibers can be evaluated within their gain regions, which is commonly absorbing for passive methods. In conclusion, the dispersion measurement with the TCFL could be of high interest for specific measurement scenarios, especially related to fiber lasers.

Acknowledgments

Financial support by the Federal Ministry of Education and Research (BMBF) (FKZ: 13N13865 and 16PGF0128) as well as the German Research Foundation (DFG: GZ JA 2611/1-1) is gratefully acknowledged.

References

[1] Fu W, Wright L G, Sidorenko P, Backus S and Wise F W 2018 *Opt. Express* **26** 9432–63
[2] Chong A, Wright L G and Wise F W 2015 *Rep. Prog. Phys.* **78** 113901
[3] Chong A, Buckley J, Renninger W and Wise F 2006 *Opt. Express* **14** 10095–100
[4] Zhang H, Tang D, Zhao L, Bao Q, Loh K P, Lin B and Tjin S C 2010 *Laser Phys. Lett.* **7** 591
[5] Balciunas T, Fourcade-Dutin C, Fan G, Witting T, Voronin A, Zheltikov A, Gerome F, Paulus G, Baltuska A and Benabid F 2015 *Nat. Commun.* **6** 6117
[6] Gebhardt M, Gaida C, Heuermann T, Stutzki F, Jauregui C, Antonio-Lopez J, Schulzgen A, Amezcua-Correa R, Limpert J and Tünnermann A 2017 *Opt. Lett.* **42** 4179–82
[7] Dudley J M, Genty G and Coen S 2006 *Rev. Mod. Phys.* **78** 1135
[8] Heidt A M, Hartung A, Bosman G W, Krok P, Rohwer E G, Schwoerer H and Bartelt H 2011 *Opt. Express* **19** 3775–87
[9] Jiang X, Joly N Y, Finger M A, Babic F, Wong G K, Travers J C and Russell P S J 2015 *Nat. Photon.* **9** 133–9
[10] Yamamoto T, Yoshida E, Tamura K R, Yonenaga K and Nakazawa M 2000 *IEEE Photonics Technol. Lett.* **12** 353–5
[11] Tateda M, Shibata N and Seikai S 1981 *IEEE J. Quantum Electron.* **17** 404–7
[12] Lee J Y and Kim D Y 2006 *Opt. Express* **14** 11608–15
[13] Galle M A and Qian L 2014 *IEEE Photonics Technol. Lett.* **26** 2020–2
[14] Shang H T 1981 *Electron. Lett.* **17** 603–5
[15] Dorrer C 2004 *Opt. Lett.* **29** 204–6
[16] Cohen L G and Lin C 1977 *Appl. Opt.* **16** 3136–9
[17] Cohen L G 1985 Comparison of single-mode fiber dispersion measurement techniques *Optical Fiber Communication Conf.* (Washington, DC: Optical Society of America) p TUF1
[18] Tiess T, Becker M, Rothhardt M, Bartelt H and Jäger M 2017 *Opt. Lett.* **42** 1125–8
[19] Tiess T, Becker M, Rothhardt M, Bartelt H and Jäger M 2017 *Opt. Express* **25** 26393–404
[20] Barmenkov Y O, Zalvidea D, Torres-Peiró S, Cruz J L and Andrés M V 2006 *Opt. Express* **14** 6394–9
[21] Data sheet: Corning HI 1060 (www.corning.com/media/worldwide/csm/documents/HI 1060 Specialty Fiber PDF.pdf) (Accessed: 30 July 2018)
[22] Ponzo G M, Petrovich M N, Feng X, Horak P, Poletti F, Petropoulos P and Richardson D J 2014 *Opt. Express* **22** 943–53